HOSTED BY

ELSEVIER

Available online at www.sciencedirect.com

ScienceDirect

Journal of Magnesium and Alloys 3 (2015) 173–179
www.elsevier.com/journals/journal-of-magnesium-and-alloys/2213-9567

Full Length Article

# Study on the early surface films formed on Mg-Y molten alloy in different atmospheres

A.R. Mirak [a,*], C.J. Davidson [b], J.A. Taylor [a]

[a] CAST CRC, School of Mechanical and Mining Engineering, The University of Queensland, Brisbane, QLD 4072, Australia
[b] CAST CRC, CSIRO Materials Science and Engineering, P.O. Box 883, Kenmore, QLD 4069, Australia

Received 30 November 2014; revised 6 June 2015; accepted 30 June 2015

Available online 1 October 2015

**Abstract**

In the present study, the non-isothermal early stages of surface oxidation of liquid Mg-1%Y alloy during casting were studied under UPH argon, dry air, and air mixed with protective fluorine-bearing gases. The chemistry and morphology of the surface films were characterized by SEM and EDX analyses. The results indicate a layer of smooth and tightly coherent oxidation film composed of MgO and $Y_2O_3$ formed on the molten Mg-Y alloy surface with 40–60 nm thickness under dry air. A dendritic/cellular microstructure is clearly visible with Y-rich second phases gathered in surface of the melt and precipitated along the grain/cell boundaries under all gas conditions. Under fluorine-bearing gas mixtures, the surface film was a mixed oxide and fluoride and more even; a flat and folded morphology can be seen under $SF_6$ with oxide as dominated phase and under 1, 1, 1, 2-tetra-fluoroethane, a smooth and compact surface film uniformly covering the inner surface of the bubble with equal oxide and fluoride thickness, which results in a film without any major defects. $MgF_2$ phase appears to be the key characteristic of a good protective film.


*Keywords:* Mg-Y alloy; SEM; EDX; Early surface film; Oxidation; Fluoridation

## 1. Introduction

Magnesium alloys are increasingly becoming important light-weight structural materials for the automotive and other industries as a result of their excellent properties such as high specific strength, high specific rigidity, good damping capacity and low density [1,2]. Due to the high affinity of magnesium for oxygen and the high vapor pressure of molten magnesium, it is essential to take some measures to prevent magnesium oxidization and burning during melting processes.

In order to process molten magnesium safely and efficiently, the melt is normally protected either by exclusion of oxygen (e.g. by covering with salt flux or an inert gas) or by the changing the nature of the surface oxide with a cover gas and thereby slowing the oxidation rate down to an acceptable level. The surface oxide of the melt may form a protective film over the melt surface, and the efficacy of this film varies with alloy and cover gas compositions [3,4].

Rare earths are frequently used as deliberate alloying additions to improve the properties of Mg alloys, particularly creep resistance. These heavy metals such as Y and Ce have also been proved to improve oxidation and corrosion resistance [5–14]. Several studies, which are detailed below, have been carried out on the isothermal oxidation behavior of magnesium alloys. These studies have typically focused on oxidation after many minutes or even hours and little information is available on the early stages of oxidation.

Fan et al. described how a Mg-3Y-4.5Ce alloy was able to be melted in air at 1173 K without any protection due to a dense and compact film forming [15,16]. They also indicated that good ignition–proofing and mechanical properties were realized in the Mg-Y-Ca-Zr system as well [17,18].

Wang et al. investigated the early oxidation behavior of Mg-Y alloys oxidized in pure $O_2$ at high temperatures isothermally and the results revealed that the improved oxidation resistance of the Mg-Y alloy is due to the formation of a continuous Mg-dissolving $Y_2O_3$ protective film. Furthermore, they investigated Y implantation on the surface oxidation behavior of AZ31 alloy and the experimental results indicated that after treatment, the oxidation resistance of AZ31 was significantly improved [19–22].

* Corresponding author. Material Engineering Department, University of Science and Technology of Iran, Narmak, Tehran, Iran. Tel.: +98 9388109638.
*E-mail address:* mirak@iust.ac.ir (A.R. Mirak).

http://dx.doi.org/10.1016/j.jma.2015.06.003

Wang et al. also explored the isothermal early oxidation behavior of Mg-10Gd-3Y alloy and showed that a dense and compact oxide film with a duplex structure was formed which was composed of $Gd_2O_3$ and $Y_2O_3$ and little MgO [23].

Ravi Kumar [24] studied the ignition resistance of pure Mg, AZ91 and WE43 alloys. He indicated that ignition can occur for pure Mg in the solid state whereas it requires the presence of liquid phase in the AZ91 alloy. The WE43 (Mg-Y) alloy was shown to be ignition-proof; the ignition resistance being attributed to the role of yttrium in the oxidation process. Investigations suggested that by implanting rare-earth elements (such as Y, Ce), the oxidation resistance of the substrate was increased.

Lin et al. focused on the interactive effect of Ce and Al in AZ91D and AM50 master alloy on ignition point and oxidation resistance. They found that Ce can improve the oxidation resistance due to "tightness" of the oxide film, and that as the Al content was increased, the lower will be ignition point [25].

The effect of Al and Y on the ignition and flammability of Mg alloys was studied by Prasad et al. They showed that there was smoldering and delayed ignition for Mg-1Y alloy but that there was no ignition for Mg-5Y specimen tips due to the formation of a protective surface oxide film containing Y [26].

In the present study, the early oxidation stages under non-isothermal conditions of Mg-Y alloy have been investigated in four different atmospheres: UHP (ultra high purity) argon, dry air, air/$SF_6$ mixture and air/HFC-134a mixture. Correspondingly, the morphology and features of the surface oxide films have been analyzed by optical and electron microscopy and EDX techniques. In addition the oxidation mechanisms of Mg-Y alloys were discussed. This work forms part of a broader study in which the oxidation behavior of pure Mg [27] and Mg-Nd alloys [14] under similar experimental conditions have already been reported.

## 2. Experimental procedure

Mg-1%Y alloy was prepared using commercial purity Mg (99.9 wt%) and major impurities of Al and Si each at 0.03 wt%, with Mn 0.02 wt% and pure Y in a mild steel crucible by electrical resistance furnace under the protection of an $SO_2$/air mixture. Note that this gas mix was used to avoid any possibility of contamination from residual fluorine that might happen if a more common fluorine-bearing cover gas was used at this stage. Once the Mg was molten, the pure Y ingot was added to the melt and held at a temperature of 700 ± 5 °C.

Each melt was cast into a pre-heated permanent mould (at 450 ± 10 °C) to produce a simple plate casting via a bottom gating system. The base of the casting was 14 mm thick, tapering linearly to 7 mm near the top. A disposable thin stainless steel tube (1 mm ID, 1.6 mm OD) was inserted horizontally into the base of the mould cavity. Different gases were metered, mixed and introduced through these tubes to provide a short burst of bubbles into the plate casting. Most or all of the bubbles were trapped during the solidification process. The following gas mixtures were used to create these internal bubbles: ultra-high purity (UHP) argon; industrial dry air; 3.5% $SF_6$ in dry air; and 3.5% HFC-R134a in dry air. The feed gas purities and significant impurities are as follows:

(i) UHP argon, min 99.999%, $O_2$ < 1 ppm, $H_2O$ < 2 ppm;
(ii) industrial dry air: 20.9% $O_2$. $H_2O$ typically 25 ppm;
(iii) $SF_6$: min 99.8%; $CF_4$ < 1000 ppm; $H_2O$ < 120 ppm; typical acidity (HF) 0.3 mg/kg; hydrolysable fluorides 1 mg/kg;
(iv) 1,1,1, 2 tetrafluoro ethane (HFC-R134a): min 99.5%. $H_2O$ < 10 ppm; acidity (HF) 1 ppm; other refrigerants 0.5 ppm.

For each experimental condition, four castings were made. X-ray radiography on each plate was used to make decisions about the best way of cutting the bubble specimens out of the casting. Ideal samples were considered to be the thin interfaces captured between two trapped impinging bubbles. The technique used in this work enables the production and sampling of the protective surface films generated under carefully-controlled reaction conditions.

The morphologies of the surface "oxide" films were examined using a scanning electron microscope model JEOL 6460 LA, while the chemical constituents of the films were determined using an attached energy dispersive X-ray (EDX) spectrometer with ultra-thin window suitable for light element analysis. All analyses were carried out at 12 kV.

Previous measurements of oxygen X-ray intensity in pure Mg samples [27] suggested that the local film thickness was quite variable at different locations in the entrapped bubbles. In that work, a simple semi-quantitative technique was described that adequately characterized the local film thickness. Calibration curves of Mg/O and Mg/F X-ray intensity ratios against film thickness, for various film materials, were prepared by Monte Carlo simulation of X-ray generation under an electron beam, using the Casino software package [28]. The detector efficiency for each element of interest was scaled by comparing the predicted and measured responses for known standards such as pure Mg, MgO, $CaF_2$ and dolomite. The influence of the carbon coating on the reference materials was included in the modeling, although bubble samples were not carbon coated, because the films were sufficiently thin that charge buildup was not apparent in the presence of the conductive substrate. Typical calibration curves are shown in figures 3 and 4 of Reference [27], along with a detailed description of the analytical technique adopted to determine film thickness and the film thickness limit.

## 3. Results and discussion

### 3.1. As cast microstructure

Fig. 1 presents the SEM images of the microstructure of an as-cast polished specimen of Mg-1%Y alloy. The microstructures consist of magnesium solid solution and the Y-rich compounds which are identified as Mg-Y and Y-Si as particle and rod-like shape phases respectively by EDX analyses. The Si is assumed to be trace impurity from the raw materials. Fig. 2 shows the Mg rich side of Mg-Y equilibrium phase diagram showing that up to 12 wt% Y can be present in the primary Mg solid solution. Given that permanent mould casting produces non-equilibrium conditions, it is reasonable to expect that the

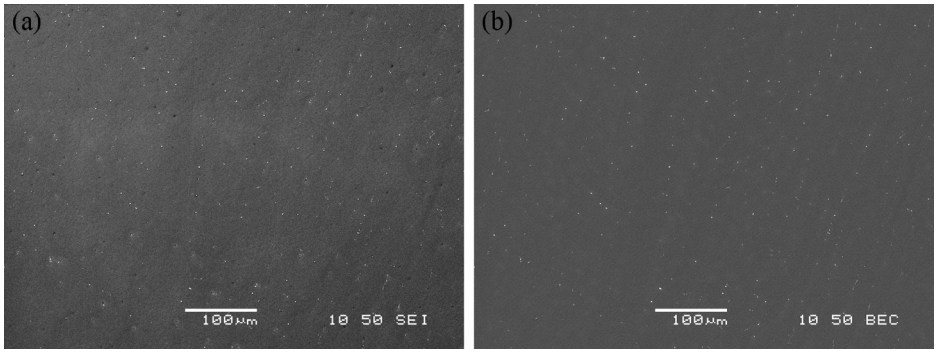


Fig. 1. (a) Secondary electron (SE) image, and (b) back scattered electron (BSE) image of the microstructure of as-polished Mg–1% Y alloy.

Mg-Y compound identified in the Mg-1%Y alloy by EDX is $Mg_{24}Y_5$.

### 3.2. X-ray analysis – qualitative

Fig. 3 shows EDX spectra from general areas representative of large fractions of the surface. The chemical characteristics of the surface film can be distinctly seen for each gas condition. As would be expected, the bubble surfaces formed under air and argon result in surfaces with the highest and lowest oxygen peaks, respectively, while fluorine was a constant feature of the bubble surfaces formed using both $SF_6$ and R134a gas mixtures. There is also a $M_\alpha$ peak of Y element present in all samples and the intensity increases in the same order as the oxygen peak (argon (lowest), $SF_6$, R134a, air (highest)).

### 3.3. Film observations under SEM

Figs. 4, 5 and 7, 8 show various SEM images of the physical structure of the surface films observed on the inner surfaces of entrapped bubbles in Mg-1%Y alloy formed under the different atmospheres. A range of macro and microstructures is apparent. The sub-surface alloy microstructure appears to be dendritic/cellular with rounded shape crystals of the Y-rich phases precipitated along the grain/cell boundaries; these structures are clearly visible beneath the compact and uniform morphology of the surface films.

#### 3.3.1. Argon

Fig. 4 shows the typical characteristics of the inner bubble surface film formed under an atmosphere of UHP argon. As can be seen, due to the thinness of the film, the inner solidification structure is clearly visible. The microstructure appears dendritic/cellular with equiaxed grains of 20–30 µm size. The solid solution forms in middle of grains and the second phases as rounded white particle and irregular shape are identified as Y-rich components consist of Mg-Y and Y-Si which precipitated along the grain boundaries as can be obvious in Fig. 4d. Due to solubility of Y element in Mg is little, the Y rich components gather on the surface of the molten alloy.

There are many pimples (similar to flower-like shape) visible on the surface and these are most likely protruding dendrites draped with oxide skin. There are also many inter granular defects as shrinkage voids and cracks that would have formed during cooling down, as shown in Fig. 4d (flash marked). There are also black particles of MgO distributed over the surface film, as obvious in BSE images (Fig. 4b). These seem to have

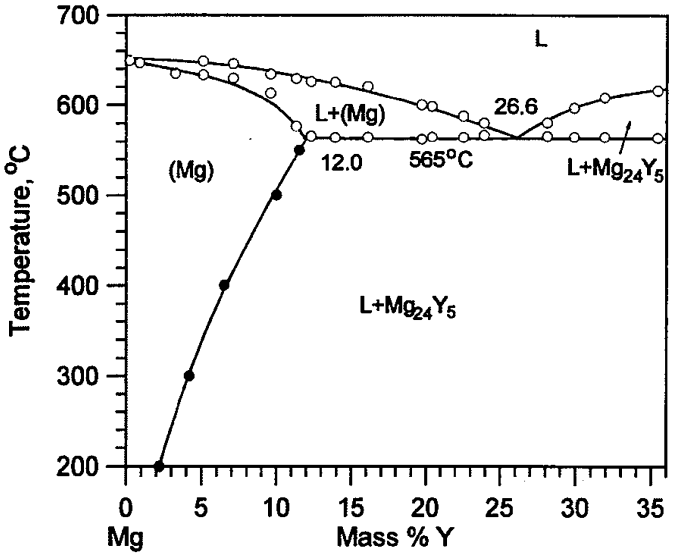


Fig. 2. Mg-rich side of the Mg-Y equilibrium phase diagram.

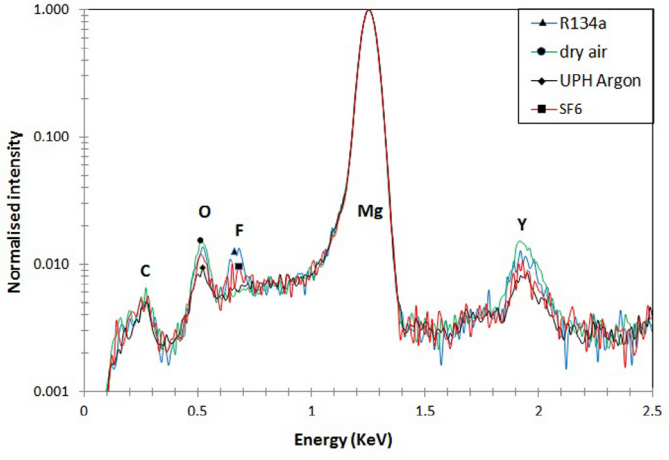


Fig. 3. Representative EDX spectra of the surface films of bubbles formed in Mg–1%Y with different bubble gas atmospheres. These spectra have been normalized to the Mg $K_\alpha$ peak.

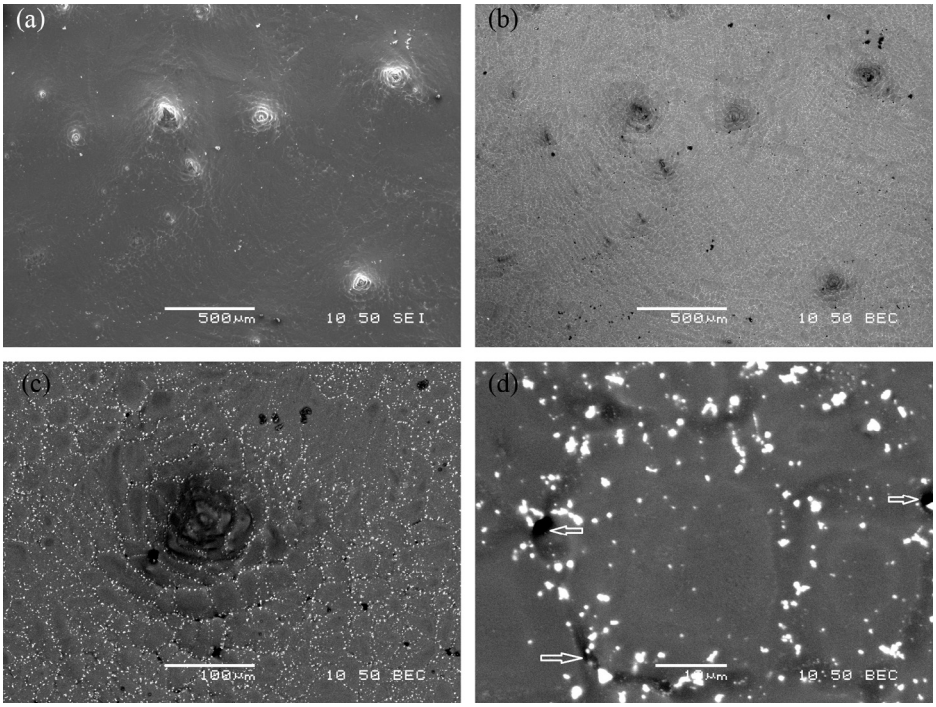


Fig. 4. SEM images of the inside surface of an entrapped argon bubble in Mg–1%Y alloy plate casting: (a) Secondary electron image of the typical microstructure; (b) a closer view of a pimple shows grain size; (c) a BSE image of the same area showing many white particles precipitated along the grain boundaries, and also some coarse black particles of MgO; (d) a closer view BSE image shows white particle morphology. Many hollows and crack defects are visible clearly.

most likely been produced during sample preparation at room temperature.

The main elements in the bulk and surface film are Mg, Y and a little oxygen. The Mg/O ratio is about 150 and this indicates that the early oxide film is 10–15 nm in thickness, calculated according to figs. 3 and 4 in Ref. [27]. The X-ray intensities from these areas are similar to those observed on freshly polished Mg and so this thickness range is assumed to represent the upper limit of subsequent oxide growth at room-temperature, between exposing the bubble and examination in the SEM.

The source of oxygen was most likely traces of air that could not be completely flushed from the inside of the steel tube prior to casting. In addition, castings were carried out during humid summer months, under conditions of relatively high ambient partial pressure of water vapor (typically 2.5–3 kPa), which could provide a further minor source of oxygen. Since the gas flow was not started until filling commenced, there would have been some diffusional exchange between the surrounding air and the argon in the outlet region of the feed pipe in those initial moments.

### 3.3.2. *Dry air*

Fig. 5 shows some of the characteristics of the inside surface of bubbles formed under industrial grade dry air. As can be seen a thick, smooth and compact surface film forms in two distinct areas: those flat, and those that occur as wrinkled bands as shown in Fig. 5. These wrinkled bands are oriented in various directions and are up to 100 µm wide and several millimeters in length. The higher Mg/O ratio in the wrinkled bands shows the

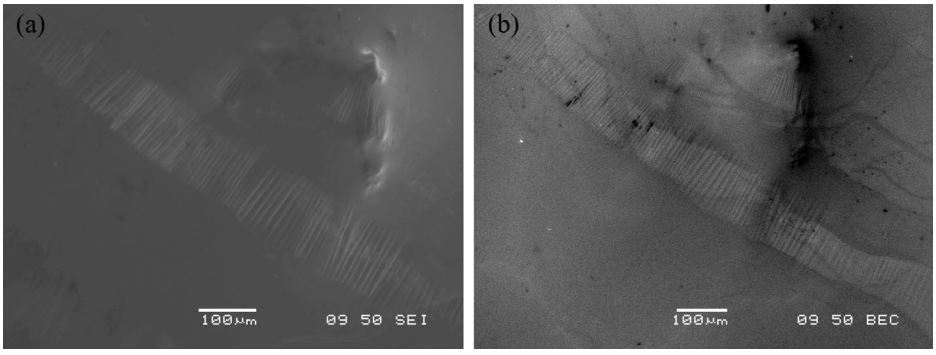


Fig. 5. SEM images of the inside surface of an entrapped dry air bubble in a Mg–1%Y alloy plate casting: (a) Secondary electron (SE) image of the general area showing the typical features, including wrinkle bands; (b) a BSE image from the same area.

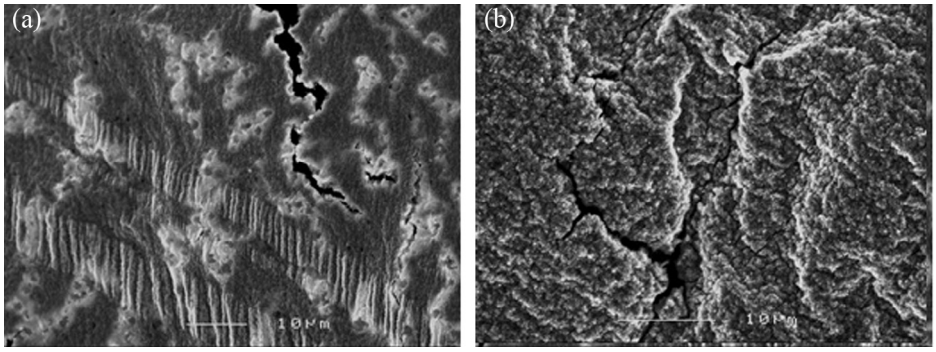


Fig. 6. SEM images of the surface film formed in pure Mg under dry air. The wrinkled and rough morphology of the oxide film is clear with many cracks and hollows present (previously unpublished images from the work reported in Ref. [27]).

thin film formed in early stage of oxidation cracks due to mechanical forces and new surface film forms in between, with the older film accommodating the associated stresses by folding.

The main elements attributed to the alloy and film are Mg, Y, and O as detected by the EDX analyses from air bubble surface. Due to Mg/O ratio measuring from surface film, the average oxide film thickness is calculated to be about 40–60 nm according to figs. 3 and 4 in Ref. [27].

A proposed mechanism of surface film forming is that due to the very high vapor pressure of Mg, there is a great deal of Mg vapor on the surface of the molten alloy and the Mg reacts with oxygen and creates MgO firstly which deposits on the melt/bubble interface. If the reaction rate is fast enough, the pressure drop will occur while there is still a liquid path to the atmosphere and oxygen fed to bubble. This is followed by enrichment of the yttrium under the layer of film, due to the limited solubility of yttrium in molten Mg alloy, as the Y level increases near the surface of the melt, $Y_2O_3$ can be form because of its lower Gibbs free energy of formation than for MgO (−1678.8 kJ/mol for $Y_2O_3$ and −517 kJ/mol for MgO [29]). At this stage $Y_2O_3$ forms prior to MgO directly from the melt, therefore the oxidation surface film consists of both MgO and $Y_2O_3$. So it seems the surface film has duplex structure and a complex oxidation process is likely to occur, as confirmed by Fan et al. in the isothermal oxidation of Mg-Y alloy [17]. In early stage of oxidation of Mg-Y alloy, it is proposed that the following reactions occur:

(1) $Y = [Y]$
(2) $2Mg + O_2 = 2MgO$
(3) $4Y + 3O_2 = 2Y_2O_3$
(4) $3MgO + 2Y = Y_2O_3 + 3Mg$

It is expected the oxide film with a smooth and compact morphology is composed of MgO and $Y_2O_3$. This stands in contrast to pure Mg that forms a loose and wrinkled morphology film of only MgO that the Pilling–Bedworth ratio (PBR) of MgO is 0.81 [30]. This is shown clearly in Fig. 6; many cracks and holes exist in the film and these can act as an easy path allowing the diffusion of $Mg^{2+}$ to further react with the inwardly mobile oxygen. Meanwhile in Mg-Y alloy, because the PB ratio of $Y_2O_3$ is greater than 1 (1.39 [30]), the formation of yttrium oxide in conjunction with MgO allows for the possibility the $Y_2O_3$ making up for the shrinkage associated with the formation of MgO such a relatively dense film is formed. In such a film, the outward movement of Mg ions and the inward movement of oxygen ions through this surface film are retarded and so it acts as a barrier to further oxidation.

### 3.3.3. *Sulphur hexafluoride, $SF_6$*

Fig. 7 shows the typical characteristics of the bubble surface film formed under an atmosphere of air containing 3.5% $SF_6$. The surface film appears fine folded and relatively uniform with many pimples without any evidence of pores. There are many bands orientated in various directions, typically of the order of 10 μm broad and several millimeters long. These bands have a wrinkled topography compared with their flatter surroundings (Fig. 7c). There are other regions however, where these bands are not evident, and the surface is relatively uniform.

The EDX analysis detected four main elements (Mg, Y, F and O) and possibly some amorphous C in the surface film and bulk in varying amounts in different areas. Oxygen:fluorine ratio in the surface film is equivalent thicknesses of independent oxide ($Y_2O_3$ and MgO) and fluoride ($MgF_2$ and $YF_3$). This is indicated that the surface film has a complex structure. The O/F intensity ratio varies from 1.4 in the flatter regions (Fig. 7a) to 2.2 in the folded areas (Fig. 7c). This indicated the oxide thickness would be expected more than fluorides.

It is possible that the presence of fluorine as a fluoride in the surface film and/or fluorine dissolved in the oxide crystals changes the surface film morphology toward higher integrity than MgO alone. This may occur by the $MgF_2$ nucleation rate changing within the MgO film and/or improved wetting between the metal and the oxide due to the presence of fluorine as suggested by Cashion [31].

### 3.3.4. *HFC-R134a*

Fig. 8 shows a dense and compact protective surface film that forms over the granular/dendritic structure under the influence of an air/3.5% R134a mixture. The surface film morphology is similar to the surface film formed in $SF_6$ with the many wrinkled bands oriented in various directions and pimple-like structures are evident at low magnification (Fig. 8a).

The EDX spectra show fluorine is present in samples prepared using the air/R134a mixture because HF and F2 are the

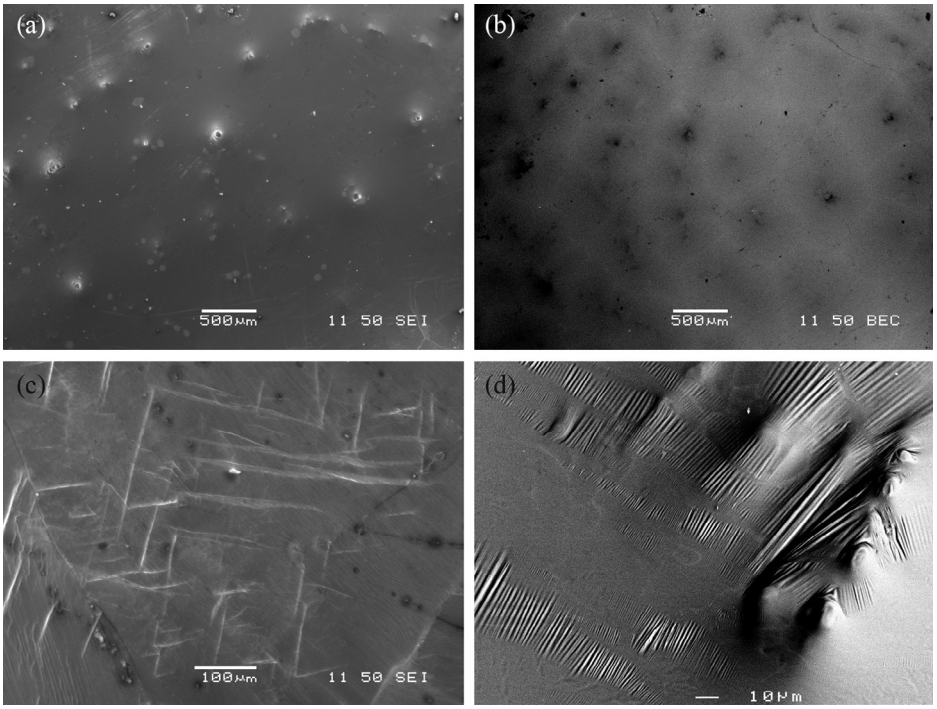


Fig. 7. SEM images of the inner surface film formed on an entrapped bubble of air/3.5%$SF_6$ mix in Mg–1% Y alloy: (a) Secondary electron image showing a general area; (b) BSE image of the same area; (c) a SE image of closer view of folded film; (d) a SE image of closer view of surface film shows many wrinkled bands.

products of HFC-134a decomposition at high temperature. Oxygen levels, on the other hand, are consistently at the same level in all of atmospheres, except for argon. The spectra show in general a very consistent O/F intensity ratio in the range 0.97–1.13, which is indicative of similar amounts of oxide and fluorides in the surface layer. The calculated value of average oxide and fluoride thickness was 30–50 nm individually according to the X-ray calibration curves (see figs. 3 and 4 in Ref. [27]).

It is also noted that due to $SF_6$ being more stable than HFC-R134a [32], so there is more fluorine found in the surface film formed under HFC-R134a cover gas. This is consistent with conversion of all fluorine in the HFC-R134a to fluorides. Furthermore, it suggests that the reaction with fluorine must be quite rapid, suppressing oxide formation at a very early stage. As with $SF_6$, the surface film is composed of oxide ($MgO/Y_2O_3$) and fluorides ($YF_3/MgF_2$) films that are stable and possibly some amorphous C and that the surface film has a complex structure.

The film composition agrees with the results presented by Liu et al. [4] after long term exposure to a similar gas composition at 760 °C. They were able to confirm $MgF_2$ using X-ray diffraction. It seems that the presence of $MgF_2$ phase in the surface film is the main reason that the film becomes dense, compact and uniform, and that the air-HFC-R134a gas mixtures can provide effective protection for molten magnesium, similar to that reported by Petersen et al. [33].

It is reported that the surface film grows via the diffusion of ions [32]. Since the outward diffusion rate of magnesium ions was much faster than that of the inward diffusion of oxygen and fluorine ions, the growth of the outer layer was controlled by the outward diffusion of $Mg^{2+}$ through the film. With a dense and

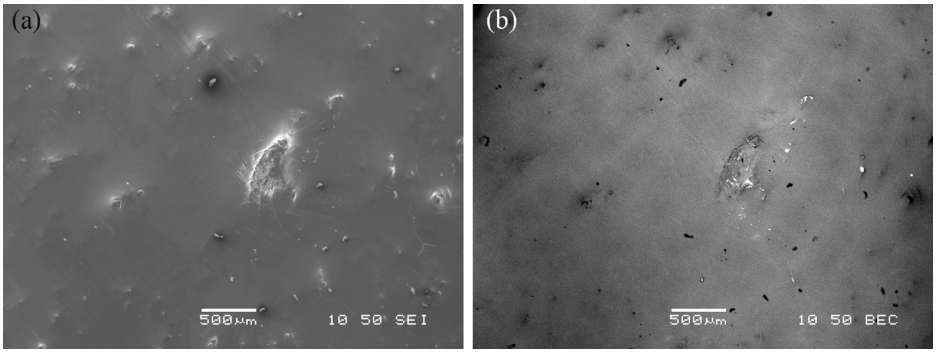


Fig. 8. SEM images of the inner surface film of entrapped bubbles of introduced air/HFC-R134a gas mixture in a Mg–1%Y plate casting: (a) Secondary electron image of the general area; (b) BSE image of (a) showing a dendritic structure.

compact film forming on the surface of molten magnesium, further oxidation was enhanced and the film had a good chemical stability. This resulted in the magnesium having excellent oxidation resistance at high temperature.

## 4. Conclusions

1. The dendritic/cellular as-cast Mg-1% Y alloy structure and the presence of fine white particles rich in Y element as the second phases precipitated along the grain boundaries.
2. The Y element and the composition of the bubble atmosphere strongly affect the characteristics of the surface film formed in pure magnesium, in terms of thickness, morphology and composition.
3. A smooth and compact protective surface film forms on surface of molten metal alloy composed of MgO and $Y_2O_3$ in early stage of oxidation of Mg-1%Y alloy at high temperature. Due to Mg/O ratio measuring from surface film, the average oxide film thickness is calculated to be about 40–60 nm according to figs. 3 and 4 in Ref. [27]. The dense morphology of this film can retard the diffusion rate of Mg and oxygen through the layer.
4. The characteristic of protective surface film formed under fluorine bearing gas mixtures is relatively smooth, compact and largely undamaged. They are mainly composed of oxide and fluoride. It seems due to the $SF_6$ is more stable than HFC-R134a and this leads to a higher concentration of fluorine in the films formed under HFC atmosphere, it is likely that the mixed oxide consist of $Y_2O_3$ and MgO is the dominate phase in surface film under $SF_6$ atmosphere.
5. The spectra from the surface film show in general a very consistent O/F intensity ratio in the range 0.97–1.13, which is indicative of similar amounts of oxide and fluorides in the surface layer under HFC atmosphere. The calculated value of average oxide and fluoride thickness was 30–50 nm individually according to the X-ray calibration curves. It is likely that the amount of $MgF_2$ phase in the surface film under HFC-R134a atmosphere is the key characteristic of a protective film.

## Acknowledgements

The authors wish to thank the Ministry of Science, Research and Technology of the Islamic Republic of Iran for the scholarship that enabled A.R. Mirak to travel to Brisbane to carry out the research program with the CAST CRC. CAST CRC was established under and is funded in part by the Australian Federal Government's Cooperative Research Centre's Scheme.

## References

[1] H. Ohara, Magnesium and Magnesium Alloy, ASM Handbook, 2004.
[2] B.L. Mordike, T. Ebert, Mat. Sci. Eng. A302 (2001) 37.
[3] J.E. Gray, B. Luan, J. Alloy. Compd. 336 (2002) 88.
[4] J.R. Liu, H.K. Chen, L. Zhao, W.D. Huang, Corros. Sci. 51 (2009) 129–134.
[5] X.Q. Zeng, Q.D. Wang, Y.Z. Lu, W.J. Ding, C. Lu, Y.P. Zhu, et al., Scripta Mater. 43 (2000) 403.
[6] G. Zhang, H. Zhang, M. Gao, D. Wei, J. Rare Earths 25 (2007) 348.
[7] J. Rao, H. Li, Int. J. Adv. Manufact. Technol. 51 (2010) 225.
[8] M. Maiss, C.A.M. Brenningkmeijer, Environ. Sci. Technol. 20 (1998) 3077.
[9] J. Wang, R. Liao, L. Wang, Y. Wu, Z. Cao, L. Wang, J. Alloy. Compd. 477 (2009) 341.
[10] J. Wang, X.R. Zhu, R. Wang, Y.D. Xu, J.J. Nie, G.P. Ling, J. Rare Earths 29 (2011) 454.
[11] J.F. Wang, P.F. Song, S. Gao, Z.Z. Shi, F.S. Pan, J. Mater. Sci. Eng. A528 (2011) 5914.
[12] M. Liu, P. Schmutz, P.J. Uggowitzer, G. Song, A. Atrens, Corros. Sci. 52 (2010) 3687.
[13] W.J. Ding, X.M. Wang, X.Q. Zeng, G.S. Wu, S.S. Yao, Y.J. Lai, Mater. Lett. 61 (2007) 1429.
[14] A.R. Mirak, C.J. Davidson, J.A. Taylor, J. Appl. Sci. Surf. 42 (2014) 826.
[15] J.F. Fan, C.H.L. Yang, G. Han, S. Fang, W.D. Yang, B.S. Xu, J. Alloys Compd. 509 (2011) 2137.
[16] J.F. Fan, G.C. Yang, Y.H. Zou, Y.H. Wei, B.S. Xu, Metal. Mater. Trans. A 40 (2009) 2148.
[17] J.F. Fan, G.C. Yang, S.L. Chen, H. Xie, M. Wang, Y.H. Zhou, J. Mat. Sci. 39 (2004) 6375.
[18] J.F. Fan, Z. Chen, W. Yang, S. Fang, B. Xu, J. Rare Earths 30 (2012) 74.
[19] X.M. Wang, X.Q. Zeng, G.S. Wu, S.S. Yao, Y.J. Lai, J. Alloy. Compd. 460 (2008) 368.
[20] X.M. Wang, X.Q. Zeng, G.S. Wu, S.S. Yao, Y.J. Lai, Appl. Surf. Sci. 253 (2007) 3574.
[21] X.M. Wang, X.Q. Zeng, G.S. Wu, S.S. Yao, Appl. Surf. Sci. 253 (2006) 2437.
[22] X.M. Wang, X.Q. Zeng, G.S. Wu, S.S. Yao, Mater. Lett. 61 (2007) 968.
[23] X. Wang, W. Weidong, T. Yongjian, X. Zeng, S. Yao, J. Alloy. Compd. 474 (2009) 499.
[24] N.V. Ravi Kumar, J.J. Blandin, M.S. Uery, E. Grosjean, Script. Mater. 49 (2003) 225.
[25] P.Y. Lin, H. Zhou, W. Li, W.P. Li, N. Sun, R. Yang, Corros. Sci. 50 (2008) 2669.
[26] A. Prasad, Z. Shi, A. Atrens, Corros. Sci. 55 (2012) 153.
[27] A.R. Mirak, C.J. Davidson, J.A. Taylor, Corros. Sci. 52 (2010) 1992.
[28] D. Drouin, A.R. Couture, D. Joly, X. Tastet, V. Aimez, R. Gauvin, Scanning 29 (2007) 92.
[29] Y.J. Liang, Y.C. Che, Handbook of Inorganic Thermodynamics Data, North-East University Press, Shenyang, 1993, p. 449.
[30] M.S. Li, High Temperature Corrosion of Metals [M], Beijing Metallurgical Industry Press, 2001.
[31] S.P. Cashion, The use of $SF_6$ for protecting molten magnesium (Ph.D. thesis), Department of Mining, Minerals and Materials Engineering, University of 399 Queensland, Australia, 1998.
[32] H. Chen, J. Liu, W. Huang, J. Mater. Sci. 41 (2006) 8017.
[33] G. Pettersen, E. Vrelid, G. Tranell, J. Fenstad, H. Gjestland, Mater. Sci. Eng. A332 (2002) 285.